

Wave packet propagation by the Faber polynomial approximation in electrodynamics of passive media

Andrei G. Borisov ^a, Sergei V. Shabanov ^{b,*}

^a *Laboratoire des Collisions Atomiques et Moléculaires, UMR CNRS-Université Paris-Sud 8625, Bât. 351, Université Paris-Sud, 91405 Orsay Cedex, France*

^b *Department of Mathematics, University of Florida, Little Hall 352, Gainesville, FL 32611, USA*

Received 18 August 2005; received in revised form 8 December 2005; accepted 9 December 2005
Available online 10 February 2006

Abstract

Maxwell's equations for propagation of electromagnetic waves in dispersive and absorptive (passive) media are represented in the form of the Schrödinger equation $i\partial\Psi/\partial t = H\Psi$, where H is a linear differential operator (Hamiltonian) acting on a multidimensional vector Ψ composed of the electromagnetic fields and auxiliary matter fields describing the medium response. In this representation, the initial value problem is solved by applying the fundamental solution $\exp(-itH)$ to the initial field configuration. The Faber polynomial approximation of the fundamental solution is used to develop a numerical algorithm for propagation of broad band wave packets in passive media. The action of the Hamiltonian on the wave function Ψ is approximated by the Fourier grid pseudospectral method. The algorithm is global in time, meaning that the entire propagation can be carried out in just a few time steps. A typical time step Δt_F is much larger than that in finite differencing schemes, $\Delta t_F \gg \|H\|^{-1}$. The accuracy and stability of the algorithm is analyzed. The Faber propagation method is compared with the Lanczos–Arnoldi propagation method with an example of scattering of broad band laser pulses on a periodic grating made of a dielectric whose dispersive properties are described by the Rocard–Powels–Debye model. The Faber algorithm is shown to be more efficient. The Courant limit for time stepping, $\Delta t_C \sim \|H\|^{-1}$, is exceeded at least in 3000 times in the Faber propagation scheme.

© 2006 Elsevier Inc. All rights reserved.

Keywords: Maxwell's equation; Time-domain algorithms; Fabers polynomial approximation; Global propagation methods; Photonics; Gratings

1. Introduction

Many time-domain algorithms for numerical simulations of the broad band wave packet propagation in electrodynamics of passive media and/or quantum mechanics use a time stepping, that is, given a configuration of the system at time t , a time-domain algorithm produces the system configuration at time $t + \Delta t$, where the time step Δt is determined by conditions resulting from the algorithm stability and required accuracy. For

* Corresponding author. Tel.: +1 352 392 8714; fax: +1 352 392 8357.

E-mail addresses: borisov@lcam.u-psud.fr (A.G. Borisov), shabanov@phys.ufl.edu (S.V. Shabanov).

instance, in a finite differencing approach, such as, e.g., the classical leapfrog scheme, the time step is bounded from above by the stability condition (the Courant limit), $\Delta t \leq \Delta t_C$. The upper bound Δt_C is typically determined by the time a signal needs to propagate through an elementary cell of the spatial grid, which is by several orders of magnitude smaller than the total propagation time [1]. There is a class of problems in numerical electromagnetism where the wave packet dynamics at intermediate times is not of significant interest, but rather the final state is important. Computing the scattering matrix would give one such example. A related and more sophisticated example would be simulations of the broad band wave packet propagation in random media [2]. To obtain a numerical solution of the initial-value problem in this case, the propagation must be carried out multiple times for every (random) state of the medium in order to perform the statistical averaging over the medium states. Clearly, a global time-domain algorithm ($\Delta t \gg \Delta t_C$) would be of great help in reducing computational costs.

The present work offers a global time-domain algorithm for solving initial value problems for Maxwell's equations for passive media whose dispersive and absorptive properties can be described by suitable Lorentz, or Rocard–Powells–Debye, or Drude models. The basic idea of our approach can be summarized as follows. In Section 2, the Maxwell equations are cast in the form of the Schrödinger equation

$$i \frac{\partial \Psi}{\partial t} = H \Psi, \quad (1.1)$$

where Ψ is a multidimensional vector field whose components are electromagnetic fields and a set of auxiliary fields that describe the medium response to applied electromagnetic fields (e.g., the medium polarization), and H is a linear differential operator that depends on the medium dispersive and absorptive properties. Its spectrum is real if no attenuation is present, and has a negative imaginary part otherwise. The squared L_2 norm of Ψ is proportional to the electromagnetic energy of the wave packet.

If Ψ_0 is the initial wave packet configuration, then $\Psi(t)$ can be found by using the fundamental solution of Eq. (1.1)

$$\Psi(t) = e^{-itH} \Psi_0. \quad (1.2)$$

Given some (grid) approximation of the spatial dependence of H and Ψ , Eq. (1.2) provides a numerical solution of the initial value problem. In what follows the same letters are used for spatial continuum and grid representations of the Hamiltonian and wave functions, unless noted otherwise. An exact solution of the initial value problem is understood here in the sense of (1.2) where H is a finite matrix obtained from the continuous Hamiltonian by means of a suitable, sufficiently accurate, spatial (grid) representation.

If H can be directly diagonalized, then (1.2) gives an exact solution for any value of $t > 0$. But this is precisely what one wants to avoid in numerical simulations because the matrix H is typically huge and the direct diagonalization is too expensive, if impossible at all. For this reason, time domain algorithms use the semi-group property of the fundamental solution: $\exp(-itH) = [\exp(-i\Delta t H)]^N$, where $\Delta t = t/N$ with an integer N being the number of time steps. For a sufficiently small time step Δt , typically, $\Delta t \sim \|H\|^{-1}$, where $\|H\|$ is the (matrix) norm of H , the action of the infinitesimal evolution operator $\exp(-i\Delta t H)$ on the state vector Ψ can be approximated by various means that do not require any direct diagonalization of H .

Section 3 is devoted to an algorithm that involves neither a direct diagonalization of H nor many time steps. It is based on the well known approximation of an analytical function by the Faber polynomial series [3] (see also the textbooks [4]). The Faber approximation method has been applied to quantum scattering problems [5] to compute the causal Green's function for the Schrödinger equation. The Faber polynomial approximation of the exponential of a non-Hermitian operator has also been used to solve the initial value problem for the Liouville–von Neumann equation that describes the time evolution of the density matrix in statistical systems [6,7]. In the case when the spectrum of H is real, the approximation yields the well known Chebyshev propagation method that has been developed to study wave packet dynamics in quantum systems [8–10] and later used in electrodynamics of non-dispersive media [11].

We apply the Faber propagation scheme to solve initial value problems in electrodynamics of passive media reformulated in the form of the Schrödinger equation (1.1) with a non-Hermitian Hamiltonian,

$$\Psi(t + \Delta t_F) = e^{-i\Delta t_F H} \Psi(t) \approx \sum_{k=0}^n c_k(\Delta t_F) F_k(H) \Psi(t). \quad (1.3)$$

Here $c_k(\Delta t_F)$ are the expansion coefficients and $F_k(H)$ are Faber polynomials. The action of $F_k(H)$ on $\Psi(t)$ can be computed recursively. The recursion relation depends on the choice of the family of Faber polynomials. The latter, in turn, is motivated by spectral properties of H . An important point to note is that the expansion (1.3) gives an accurate approximation for the fundamental solution for large values of $\Delta t_F \gg \Delta t_C \sim \|H\|^{-1}$ and, hence, the propagation can be done in just a few time steps. The Faber series (1.3) is known to converge exponentially as the approximation order n increases. The accuracy of the algorithm is assessed in Section 4. In Sections 5 and 6 the algorithm is applied to scattering of broad band laser pulses on a dielectric grating. Dispersive properties of the grating material are described by the Rocard–Powles–Debye model with a single pole. The frequency band of the initial pulse is chosen to cover the anomalous dispersion range (the pole) of the dielectric. The Faber propagation scheme is shown to be more efficient than the Lanczos–Arnoldi propagation scheme applied earlier to the same system [12]. The Courant limit can be exceeded in at least 3000 times, $\Delta t_F \geq 3000\Delta t_C$. Due to the exponential convergence of the algorithm it can be used as a benchmark for testing various time propagation schemes. Note also that it can be applied with any suitable finite-dimensional approximation of the Hamiltonian H (finite elements, or finite differencing, or any spectral representation). In our simulations, the Fourier grid pseudospectral representation of H has been used [13,14].

2. Maxwell equations in the Hamiltonian form

Let \mathbf{D} and \mathbf{B} be electric and magnetic inductions, respectively, and \mathbf{E} and \mathbf{H} the corresponding fields. When no external currents and charges are present, the dynamical Maxwell’s equations read

$$\dot{\mathbf{D}} = c\nabla \times \mathbf{H}, \quad \dot{\mathbf{B}} = -c\nabla \times \mathbf{E}. \tag{2.1}$$

The over-dot denotes the partial derivative with respect to time, and c is the speed of light in the vacuum. Eq. (2.1) have to be supplemented by the Gauss law $\nabla \cdot \mathbf{D} = 0$ and also by $\nabla \cdot \mathbf{B} = 0$. Relations between the fields and inductions are determined by physical properties of the medium in question.

As an example we consider the Rocard–Powles–Debye model dielectric (the ionic crystal model [15,16]) with one resonance, which is used in our numerical simulations. The case with multiple resonances can be studied in a similar fashion. In this model $\mathbf{H} = \mathbf{B}$, and the Fourier harmonics of the electric field and induction of frequency ω are related by $\mathbf{D}(\omega) = \varepsilon(\omega)\mathbf{E}(\omega)$ where the dielectric constant is given by

$$\varepsilon(\omega) = \varepsilon_\infty + \frac{(\varepsilon_0 - \varepsilon_\infty)\omega_T^2}{\omega_T^2 - \omega^2 - i\eta\omega}, \tag{2.2}$$

with $\varepsilon_{\infty,0}$ being constants, ω_T the resonant frequency, and η the attenuation. Let \mathbf{P} be the dispersive part of the total polarization vector of the medium. Then $\mathbf{D} = \varepsilon_\infty\mathbf{E} + \mathbf{P}$. By using the Fourier transform, it is straightforward to deduce that \mathbf{P} satisfies the second-order differential equation

$$\ddot{\mathbf{P}} + \eta\dot{\mathbf{P}} + \omega_T^2\mathbf{P} = \varepsilon_\infty\omega_p^2\mathbf{E}, \tag{2.3}$$

where $\omega_p^2 = (\varepsilon_0 - \varepsilon_\infty)\omega_T^2/\varepsilon_\infty$ if $\varepsilon_0 - \varepsilon_\infty$ is positive, otherwise, $\omega_p^2 \rightarrow -\omega_p^2$ in (2.3). Eq. (2.3) must be solved with zero initial conditions, $\mathbf{P} = \dot{\mathbf{P}} = 0$ at $t = 0$.

Define a set of auxiliary fields $\mathbf{Q}_{1,2}$ by $\mathbf{P} = \sqrt{\varepsilon_\infty}\omega_p\mathbf{Q}_1/\omega_T$ and $\dot{\mathbf{Q}}_1 = \omega_T\mathbf{Q}_2$. Maxwell’s equations and (2.3) can be written as the Schrödinger equation (1.1) in which the wave function and the Hamiltonian are defined by

$$\Psi = \begin{pmatrix} \varepsilon_\infty^{1/2}\mathbf{E} \\ \mathbf{B} \\ \mathbf{Q}_1 \\ \mathbf{Q}_2 \end{pmatrix}, \quad H = \begin{pmatrix} 0 & ic\varepsilon_\infty^{-1/2}\nabla \times & 0 & -i\omega_p \\ -ic\nabla \times \varepsilon_\infty^{-1/2} & 0 & 0 & 0 \\ 0 & 0 & 0 & i\omega_T \\ i\omega_p & 0 & -i\omega_T & -i\eta \end{pmatrix}. \tag{2.4}$$

Here $\varepsilon_{\infty,0}$ are set to one in the vacuum, and to some specific values in the medium in question. The squared L_2 norm of the wave function is proportional to the total electromagnetic energy of the wave packet. When attenuation is not present, $\eta = 0$, the Hamiltonian is Hermitian relative to the conventional L_2 scalar product, and the norm (or energy) is conserved.

In our simulations, an absorbing layer of a conducting medium has been introduced at the grid boundaries to prevent reflections of the wave packet. The conductivity σ of the layer depends on position. The induced current in a conducting media has the form $\sigma \mathbf{E}$. Hence, in the presence of the conducting layer the Hamiltonian (2.4) is modified by inserting $-4\pi i \sqrt{\varepsilon_\infty} \sigma$ in place of zero in the upper-right corner. Further details can be found in our earlier works [17,18,12].

3. Faber polynomial propagation scheme

Let D be a bounded, closed continuum in the complex plane such that the complement of D is simply connected in the extended complex plane and contains the point at $z = \infty$ (e.g., a polygon, an ellipse, etc.). By the Riemann mapping theorem [4], there exists a conformal mapping ξ which maps the complement of a closed disk with center at the origin and radius ρ onto the complement of D , satisfying the normalization condition, $\xi(w)/w \rightarrow 1$ as $|w| \rightarrow \infty$. Then its Laurent expansion at ∞ is given by

$$\xi(w) = w + \sum_{k \geq 0} \gamma_k w^{-k}. \quad (3.1)$$

The radius ρ of the disk is called the logarithmic capacity of D . This quantity plays an important role in the accuracy analysis given below. The family of Faber polynomials F_k associated with a conformal mapping ξ is defined via the recursion relation

$$F_{k+1}(z) = zF_k(z) - \sum_{j=0}^k \gamma_j F_{k-j}(z) - k\gamma_k, \quad F_0(z) = 1. \quad (3.2)$$

For a function $f(z)$ that is analytic at every point of D , the Faber series

$$f(z) = \sum_{k=0}^{\infty} c_k F_k(z)$$

is defined by

$$c_k = \frac{1}{2\pi i} \int_{|w|=R} \frac{f(\xi(w))}{w^{k+1}} dw, \quad (3.3)$$

where $R > \rho$ is sufficiently small that f can be extended analytically to the contour Γ_R being the image of the circle $|w| = R$ under the conformal mapping ξ . The value $R = \rho$ is acceptable if ξ can be extended continuously to the circle $|w| = \rho$ (e.g., when the boundary of D is a closed simple curve with no self-intersections (a Jourdan curve)). The Faber series converges uniformly and absolutely to f on every region bounded by Γ_R to which f can be extended analytically [19]. This theorem establishes mathematical foundations for the Faber polynomial approximation (1.3) of the fundamental solution of (1.1).

The Faber polynomial algorithm for solving initial value problems for (1.1) is as follows. First, choose a (Jourdan) contour Γ that encloses the spectrum of H . Some criteria for choosing such a contour are discussed in the following section. Second, find the corresponding conformal mapping ξ . In particular, if Γ is a polygon, this task can be accomplished by the Schwartz–Christoffel transformation. For complicated polygons, there is a numerical algorithm to do so [20]. Next, the Faber expansion coefficients $c_k(\Delta t_F)$ are computed by means of (3.3) where $f(z) = \exp(-i\Delta t_F z)$. The action of the Faber polynomials of H on $\Psi(t)$ in (1.3) is computed using the recursion relation (3.2). Let $\Phi_k = F_k(H)\Psi(t)$. Then

$$\Phi_{k+1} = (H - k\gamma_k)\Phi_k - \sum_{j=0}^k \gamma_j \Phi_{k-j}, \quad (3.4)$$

where $\Phi_0 = \Psi(t)$ and $\Phi_1 = (H - \gamma_0)\Phi_0$. The series (1.3) converges uniformly on the entire spectral range of H . In order to make the algorithm memory friendly, it is desired to make the sequence of γ_k not only finite, but also as short as possible. In Section 5, we apply this algorithm to the Hamiltonian (2.4) and choose an ellipse to enclose its spectrum.

From the numerical point of view, the recursion relation (3.4) is, in general, unstable because the minimax norm of Faber polynomials grows rapidly as their order increases, $\max_D |F_k(z)| \leq 2\rho^k$ (see [21]). In other words, the norm of Φ_k would grow exponentially, while the decay of $c_k(\Delta t_F)$ still provides the convergence of (1.3). However, in a numerical implementation of (3.4), one might encounter floating point exceptions with a subsequent loss of accuracy. To avoid this instability, the Hamiltonian H must be scaled so that its spectrum lies in the domain whose logarithmic capacity is one. If β is the scaling factor, then $\exp(-i\Delta t_F H) = \exp(-i\Delta t_s H_s)$, where $H_s = H/\beta$ and $\Delta t_s = \beta\Delta t_F$. Thus, in the recursion relation (3.4) the scaled Hamiltonian H_s and the sequence γ_k generated by the conformal mapping (3.1) with $\rho = 1$ must be used, while the expansion coefficients in the Faber series (1.3) are determined by

$$c_k(\Delta t_s) = \frac{1}{2\pi} \int_0^{2\pi} \exp[-i\Delta t_s \zeta(e^{i\varphi})] e^{-ik\varphi} d\varphi. \tag{3.5}$$

Note that the exponential $f(z) = \exp(-i\Delta t_s z)$ is an analytic function in the entire complex plane so that, assuming Γ to be a Jourdan curve, one can set $R = \rho$ in (3.3) and use the fact that the spectrum of the scaled Hamiltonian lies in a domain with $\rho = 1$ and therefore $w = e^{i\varphi}$ in (3.3). Clearly, the scaling factor β must be chosen as small as possible to allow for larger time steps $\Delta t_F = \Delta t_s/\beta$.

4. Accuracy and efficiency assessment

The range R_H of H is a set of complex numbers $(\Psi, H\Psi)/\|\Psi\|^2$ obtained for all normalizable wave functions Ψ . Here (\cdot, \cdot) denotes a scalar product, and $\|\cdot\|$ is the norm associated with it. The norm of the resolvent of H is bounded by [22]

$$\|(z - H)^{-1}\| \leq [d(z, R_H)]^{-1}, \tag{4.1}$$

where $d(z, z') = |z - z'|$ is the distance on the complex plane, and the distance between z and a set R_H is defined as $\min_{z' \in R_H} d(z, z')$. Let Γ be any closed (Jourdan) curve enclosing the spectrum of H . Let P_n be a polynomial of order n that is used to approximate the fundamental solution of (1.1), that is, $\exp(-itH)\Psi_0 \approx P_n(H)\Psi_0$. By making use of the Cauchy theorem, it is straightforward to see that the accuracy of the approximation is bounded by

$$\|\exp(-itH)\Psi_0 - P_n(H)\Psi_0\| = \left\| \frac{1}{2\pi i} \int_{\Gamma} \frac{e^{-itz} - P_n(z)}{z - H} \Psi_0 dz \right\| \leq C_{\Gamma} \|\Psi_0\| \max_{z \in \Gamma} |e^{-itz} - P_n(z)| \equiv \epsilon_n(\Gamma) \|\Psi_0\|, \tag{4.2}$$

where the constant $C_{\Gamma} = L_{\Gamma}/[2\pi d(\Gamma, R_H)]$ and L_{Γ} is the length of Γ . To find C_{Γ} , Eq. (4.1) has been used. Note that C_{Γ} depends on H and Γ , but is independent of the approximation order n . Hence, it follows from (4.2) that the error of the polynomial approximation of the solution of the initial value problem for (1.1) can be made as small as desired because the Faber polynomial approximation $P_n(z)$ converges to $\exp(-itz)$ absolutely and uniformly in D .

In addition, it is worth noting that the Faber polynomial approximation provides the so called “near best” polynomial approximation of an analytic function. By definition, $\|f\|_{\infty} = \max_{z \in D} |f(z)|$. The maximum principle for analytic functions states [4] that if f is analytic in D and continuous in the closure of D , then $|f|$ cannot attain its maximum at interior points of D . According to (4.2) and the maximum principle for functions analytic in D bounded by Γ , the accuracy $\epsilon_n(\Gamma)$ of a polynomial approximation of an analytic function f of a matrix H (in our case, $f(z) = \exp(-itz)$) is

$$\epsilon_n(\Gamma) = C_{\Gamma} \|e^{-itz} - P_n(z)\|_{\infty}. \tag{4.3}$$

The fundamental theorem for polynomial approximations of functions analytic in the interior of D and continuous in D states that there exists a unique best minimax polynomial approximation P_n^f to f , that is, [23]

$$\|f - P_n^f\|_{\infty} \leq \|f - P_n\|_{\infty} \tag{4.4}$$

for any polynomial P_n of order n . In practice, it is not easy to find P_n^f . Suppose we choose some polynomial approximation, that is, we define a projection operator $\mathcal{P}_n f = P_n$. In particular, for Faber polynomials

$\mathcal{P}_n = \mathcal{P}_n^F$, and $\mathcal{P}_n^F f$ is given by the truncated Faber series. Then it follows from the identity $f - \mathcal{P}_n f = f - P_n^f + \mathcal{P}_n(P_n^f - f)$ that

$$\|f - \mathcal{P}_n f\|_\infty \leq (1 + \|\mathcal{P}_n\|)\|f - P_n^f\|_\infty. \quad (4.5)$$

Thus, our polynomial approximation appears to be “near best”, provided the norm of the projection operator \mathcal{P}_n is not so large. For Faber polynomials, one can show that [23,24]

$$\|\mathcal{P}_n^F\| \leq \frac{V}{\pi} \left(\frac{4}{\pi^2} \ln n + B \right) \quad (4.6)$$

for $n \geq 1$. Here $B \approx 1.773$ and $V = \int_\Gamma |d\theta(z)| \geq 2\pi$ and $\theta(z)$ is the angle that is made by a line tangent to Γ with the positive real axis. For a convex D , $V = 2\pi$ by the Radon theorem. In our simulations, D is an ellipse, which is convex, therefore

$$\|\mathcal{P}_n^F\| < 9, \quad n \leq 835. \quad (4.7)$$

Eq. (4.7) shows that by using the Faber polynomial approximation to f we do not lose more than one decimal place in accuracy as compared with the best minimax polynomial approximation. In this case, one can also show that [4]

$$\|f - \mathcal{P}_n^F f\|_\infty \leq \frac{(\rho/R)^{n+1} V}{\pi(1 - \rho/R)} \max_{z \in \Gamma_R} |f(z)|, \quad (4.8)$$

for any domain bounded by Γ_R , $R > \rho$, to which f can be extended analytically. Thus, the Faber series (1.3) converges exponentially as the approximation order n increases. From (4.8) some basic principles for choosing the contour Γ follow.

First, because of the exponential convergence of the Faber series, it is desired to make the logarithmic capacity ρ as small as possible. Alternatively, if ρ is set to one, the scaling factor β must be as small as possible, that is, the contour should enclose the spectrum of H as tight as possible. In principle, if the structure of the spectrum of H (or, at least, its range) is roughly known, one can find a polygon that tightly encloses the spectrum. The corresponding conformal mapping can be computed numerically [20]. The unfortunate feature of this approach is that the infinite Laurent series (3.1) is required. Hence, the recursion relation (3.4) becomes memory unfriendly in numerical simulations: All the preceding Φ_k must be kept in the operational memory. Thus, when choosing the contour, one should compromise between the approximation order and the memory use efficiency of the algorithm [5].

Second, if possible, the contour Γ should not go too far into the upper part of the complex plane to avoid the exponential growth of the factor $\max_\Gamma |\exp(-i\Delta t_s z)|$ and to allow for larger time steps. Note that the necessary accuracy can still be reached, even if the contour goes through the upper part of the complex plane, by increasing the approximation order n . The latter, however, would lead to a less efficient propagation scheme because more operations per time step are required.

5. The case of an elliptic contour

Faber polynomials associated with an elliptic contour have the simplest (shortest) recursion relation [4]. For this reason this family of the Faber polynomials have been used in many aforementioned applications in quantum and statistical mechanics. Here we use the Faber polynomials associated with an ellipse to illustrate the Faber propagation scheme in electrodynamics of passive media.

Consider Γ being an ellipse $(x - x_0)^2/a^2 + (y - y_0)^2/b^2 = 1$ where $z = x + iy$. The ellipse is an image of the circle $|w| = \rho$ under the conformal mapping

$$\zeta(w) = w + \gamma_0 + \gamma_1/w, \quad (5.1)$$

where $a = \rho + \gamma_1/\rho$, $b = \rho - \gamma_1/\rho$, and $\gamma_0 = x_0 + iy_0$ is the center of the ellipse. The logarithmic capacity of an ellipse is $\rho = (a + b)/2$ and $\gamma_1 = \rho(a - b)/2$. We choose $\rho = 1$ so that

$$\gamma_1 = 1 - b.$$

In this case, the optimization parameters are the scaling factor β and the number $b + y_0$ that determines the factor $\max_{\Gamma} |\exp(-i\Delta t_s z)| = \exp[\Delta t_s(b + y_0)]$ in the accuracy (4.8) of the Faber approximation.

The recursion relation (3.4) associated with the elliptic contour has only two terms

$$\Phi_{k+1} = (H_s - \gamma_0)\Phi_k - \gamma_1\Phi_{k-1}, \quad k > 1, \tag{5.2}$$

where $\Phi_0 = \Psi(t)$ and $\Phi_1 = (H_s - \gamma_0)\Phi_0$. The Faber expansion coefficients have the form

$$c_k(t_s) = \left(\frac{-i}{\sqrt{\gamma_1}}\right)^k e^{-i\Delta t_s \gamma_0} J_k(2t_s \sqrt{\gamma_1}). \tag{5.3}$$

Here J_k is the Bessel function. When computing the integral (3.5) we assume that $\gamma_1 > 0$ (which is consistent with the spectral properties of the Hamiltonian H used in our simulations). The exponential convergence of the Faber series can easily be seen from the exponential decay of the Bessel function for $k > 2\Delta t_s \sqrt{\gamma_1}$.

The Hamiltonian (2.4) cannot have eigenvalues with positive imaginary parts, otherwise the energy of the wave packet (the squared norm of Ψ) would increase with time, which is not possible in passive media. Hence, by physical reasons, the spectrum of the Hamiltonian lies in the lower half of the complex plane. It is also clear that the spectrum of the Hamiltonian is symmetric about the imaginary axis (for every direction in space, there are incoming and outgoing waves). Hence, we set $x_0 = 0$. The spectrum of H lies in a rectangle $[-E_m, E_m] \times [-v, 0]$ with E_m and v to be determined below. Our strategy is to find an ‘‘optimal’’ ellipse with $\rho = 1$ that contains a scaled rectangle $[-E_s, E_s] \times [-v_s, 0]$, where $E_s = E_m/\beta$ and $v_s = v/\beta$.

First, we determine the bounds, E_m and v , on the spectral range of H . Let $z_\psi = (\Psi, H\Psi)/\|\Psi\|^2$ be a point in R_H . Let $H = H_0 - iV$ where $H_0 = (H + H^\dagger)/2 = H_0^\dagger$ and $V = i(H - H^\dagger)/2 = V^\dagger$ is positive semidefinite. Then

$$E_m = \max_{\psi} \operatorname{Re} z_\psi = \max_{\psi} (\Psi, H_0 \Psi) / \|\Psi\|^2 = \|H_0\|. \tag{5.4}$$

Thus, E_m is the maximal eigenvalue of H_0 because H_0 is Hermitian. It can be found by the standard numerical procedure. If $\Psi_n = H_0 \Psi_{n-1}$ for $n = 1, 2, \dots$ for some initial vector Ψ_0 , the sequence $\|\Psi_n\|/\|\Psi_{n-1}\|$ converges to the maximal eigenvalue E_m of H_0 as n increases. A rough estimate for E_m can also be obtained by noting that the maximal wave vector supported by the grid in the Fourier pseudospectral representation is $k_{\max} = \pi/a_{\min}$ with a_{\min} being the smallest grid step (if a non-uniform grid is used). Hence, $E_m \approx ck_{\max}$. Similarly,

$$v = \max_{\psi} (-\operatorname{Im} z_\psi) = \max_{\psi} (\Psi, V \Psi) / \|\Psi\|^2 = \max\{4\pi\sqrt{\varepsilon_\infty} \sigma_{\max}, \eta\} = 4\pi\sqrt{\varepsilon_\infty} \sigma_{\max}, \tag{5.5}$$

where σ_{\max} is the maximal value of conductivity of the absorbing layer. Here we have used that fact that V is diagonal and the medium attenuation η is small compared to σ_{\max} .

By the symmetry, the center of the ellipse is set to coincide with the center of the rectangle,

$$\gamma_0 = -iv_s/2.$$

An ellipse that contains the rectangle vertices should satisfy the following condition:

$$\frac{a}{b} = \frac{E_s}{\sqrt{b^2 - |\gamma_0|^2}}. \tag{5.6}$$

Since $\rho = 1$, $a = b - 2$. Eq. (5.6) relates b and the scaling factor β .

As has been argued above, to increase the time step $\Delta t_F = \Delta t_s/\beta$, the scaling factor β must be minimal. So, one can take b for which β attains its minimal value. The smallest β is reached when

$$\frac{b}{a} = \left(\frac{|\gamma_0|}{E_s}\right)^{2/3} = \left(\frac{v}{2E_m}\right)^{2/3}. \tag{5.7}$$

Observe that if $v = 0$, that is, if the spectrum of H is real, the optimal ellipse has $b = 0$ and $\beta = E_m$. In this case, the Faber polynomial series is nothing but the Chebyshev polynomial series. Unfortunately, when $v \neq 0$ by making β smaller we increase the number $b + y_0$. Hence, the ellipse gets farther into the upper half of the complex plane and higher orders of the Faber approximation are needed to achieve desired accuracy according to

(4.8). So, in our simulations we take β larger than its minimal value and thereby reduce $b + y_0$ by making b smaller (see following section for details).

6. Applications to nanostructured periodic materials

As an example of possible applications of the present method to photonics, the Faber propagation scheme associated with an elliptic contour is applied to scattering of broad band wave packets on nanostructured periodic materials, the subject of current interest in photonics [25]. We consider a grating made of a periodic array of ionic crystal cylinders in vacuum. This system has been previously studied by the Lanczos–Arnoldi time propagation scheme [12]. In particular, the role of trapped modes (guided wave resonances) and polaritonic excitations in transmission and reflection properties of the grating in the infrared range has been elucidated. Apart from illustrating the Faber propagation scheme, our primary interest is to compare its efficiency with the efficiency of the Lanczos–Arnoldi propagation scheme.

The geometry of the system is sketched in the inset of Fig. 2. The system has a translation symmetry along one of the Euclidean axes, chosen to be the y -axis. It is periodic along the x -axis with period D_g , while the z -direction is transverse to the grating. The packing density $R/D_g = 0.1$, where R is the radius of cylinders and $D_g = 10.8 \mu\text{m}$ is the grating period. The broad band wave packet is represented by a Gaussian pulse that is about 38 fs long and has the carrier frequency of 173 meV. It propagates along the z -axis and is linearly polarized with the electric field oriented along the y -axis, i.e., parallel to the cylinders (the so called TE polarization). The spectrum of the wave packet is concentrated in a wavelength domain $\lambda \geq D_g$ such that the scattering is dominated by the zero diffraction mode (the reflected and transmitted beams propagate mainly along the z -axis). A change of variables is used in both x ($x = f_1(x_1)$) and z ($z = f_2(x_2)$) coordinates to enhance the sampling efficiency in the vicinity of medium interfaces so that the boundary conditions are accurately reproduced by the Fourier grid pseudospectral method. A typical size of the mesh corresponds to $-17.3D_g \leq z \leq 15.3D_g$, and $-0.5D_g \leq x \leq 0.5D_g$ with, respectively, 384 and 64 mesh points. Note that, because of the variable change, a uniform mesh in the auxiliary coordinates (x_1, x_2) corresponds to a non-uniform mesh in the physical (x, z) space. The Lanczos–Arnoldi time propagation is carried out with a fixed time step $\Delta t_L = 0.138$ fs. The propagation by the Faber method has been done with different time steps $\Delta t_F = j\Delta t_L$, with $j = 25, 50, 100, 200, 400$, and 1000 (see below).

The dielectric function of the ionic crystal material is approximated by the single oscillator model (2.3). Following the work [15], we chose the parameters representative for the beryllium oxide: $\varepsilon_\infty = 2.99$, $\varepsilon_0 = 6.6$, $\omega_T = 87.0$ meV, and the damping $\eta = 11.51$ meV. Thus, for $D_g = 10.8 \mu\text{m}$ two types of resonances can be excited in the system within the frequency domain covered by the incident pulse. Structure resonances are characteristic for periodic dielectric gratings. They are associated with the existence of guided wave modes [26,27]. As has been demonstrated previously, in the absence of losses, structure resonances lead to 100% reflection within a narrow frequency interval(s) for wavelengths $\lambda \sim D_g$. The second type of resonances arise because of polaritonic excitations for wavelengths $\lambda \sim D_T = 2\pi c/\omega_T = 26.9 \mu\text{m}$. These are associated with substantial energy losses in the ionic crystal material. A detailed discussion of the transmission and reflection properties of this grating can be found in [12].

Fig. 1a shows the elliptic contour used in our simulations. Its logarithmic capacity is one, $\rho = 1$, and the corresponding conformal mapping (5.1) reads $\zeta(w) = w - 0.005i + 0.99/w$ so that $b = 0.01$. The scaling factor $\beta = E_m/E_s$, where $E_m = 0.6468$ and $E_s = 1.7$. The shaded area is the rectangle $[-E_s, E_s] \times [-v_s, 0]$ that contains the range of the scaled Hamiltonian $H_s = H/\beta$ as explained in Section 5. The maximum imaginary part of the scaled Hamiltonian, $v_s = 0.01$, is consistent with our choice of the absorbing layer. The order n of the Faber polynomial approximation is set by the exponential decay of the expansion coefficients (5.3). In our simulations, we demand that $|c_k|$ becomes less than 10^{-15} for $k \geq n$. The behavior of $|c_k|$ is shown in Fig. 1b for time steps $\Delta t_F = j\Delta t_L$ with $j = 50, 200$, and 1000.

The transmitted signal is collected on the “virtual detector” located at $z_d = 3.22D_g$ behind the structure. The zero-order component of the electric field,

$$E_0(z_d, t) = \frac{1}{D_g} \int_0^{D_g} E(x, z_d, t) dx \quad (6.1)$$

is shown in Fig. 2.

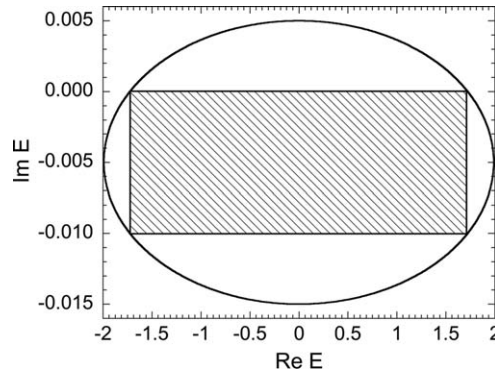


Fig. 1a. The elliptic contour used in our simulations. Results are presented on the complex plane of the scaled energy ($\text{Re } E$, $\text{Im } E$). The shaded rectangle contains the range of the scaled Hamiltonian $H_s = H/\beta$. Further details are given in the text.

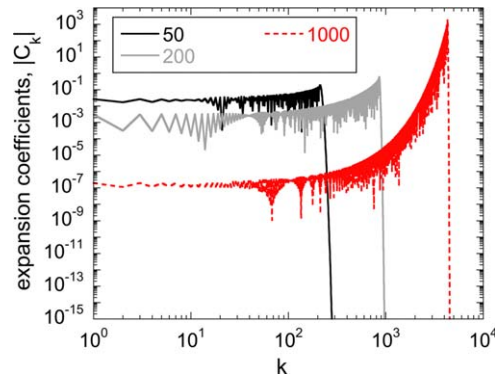


Fig. 1b. The log–log plot of absolute values $|c_k|$ of the expansion coefficients versus k for time steps $\Delta t_F = j\Delta t_L$ with $j = 50, 200,$ and 1000 as indicated in the inset of the figure.

The existence of a trapped mode (resonance) can easily be inferred from the temporal evolution of the electromagnetic field. The main transmitted pulse is clearly visible. It has a significant amplitude and a duration about 38 fs. After the main pulse passes the array, it leaves behind excited quasistationary modes which loose

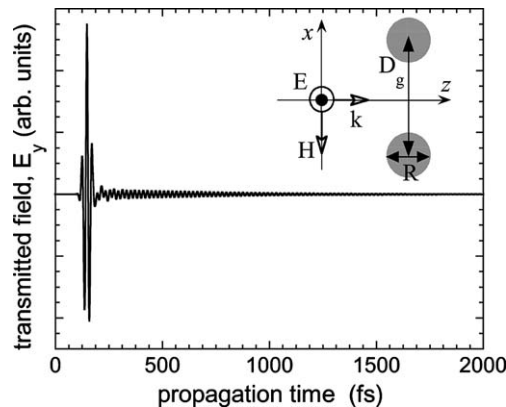


Fig. 2. Electric field of the zero-order transmitted wave as a function of time measured in femtoseconds. The signal is registered by a detector placed behind the periodic layer of ionic crystal cylinders. The grating geometry is sketched in the inset of the figure.

their energy by radiating almost monochromatic waves. By symmetry, the same radiation of quasistationary modes is registered in the reflection direction by a detector placed in front of the layer (not shown here). The quasistationary mode associated with polaritonic excitations in the ionic crystal has a wave length $\lambda \sim D_T$ and is short-lived due to the strong absorption of the material at the resonance (the anomalous dispersion region). Therefore the observed lasing effect is mainly due to the long-lived structure resonance at $\lambda \sim D_\rho$. The radiation of this mode appears as exponentially damped oscillations coming after the main signal. The exponential decay due to a finite lifetime of the quasi-stationary mode is clearly seen. The resonance lifetime is in the picosecond range, i.e., a thousand times longer than the initial pulse duration. For lossless media, the existence of the quasistationary mode(s) leads to a 100% reflection at the resonant frequency, as has been discussed in detail in Refs. [12,28]. Finally, the concept of trapped modes localized on successive layers and interacting with each other provides a theoretical framework for light propagation in layered structures such as photonic crystal slabs [29].

The main results of the paper are summarized in Fig. 3 and Table 1 where we show the precision of the Faber propagation scheme and compare its numerical costs with those of the Lanczos–Arnoldi scheme. Fig. 3 presents a relative error of the time propagation, defined as $|\{E_0(z_d, t) - E_{\text{ref}}(z_d, t)\}/E_{\text{ref}}(z_d, t)|$, where the reference signal $E_{\text{ref}}(z_d, t)$ is chosen to be the result obtained by the Faber propagation scheme with $\Delta t_F = 50\Delta t_L$. The choice is motivated by a higher precision of the Faber scheme (thanks to its exponential convergence) and by the fact that the factor $\max_T |\exp(-i\Delta t_F z)|$ is minimal for the smallest Δt_F used in our simulations. There is no change in Fig. 3 if the reference field is computed with $\Delta t_F = 25\Delta t_L$ or $\Delta t_F = 50\Delta t_L$ (see below).

It follows from our results that the Faber propagation scheme has a higher accuracy than the Lanczos–Arnoldi propagation at reduced computational costs. The error was saturated at 10^{-10} value when 10

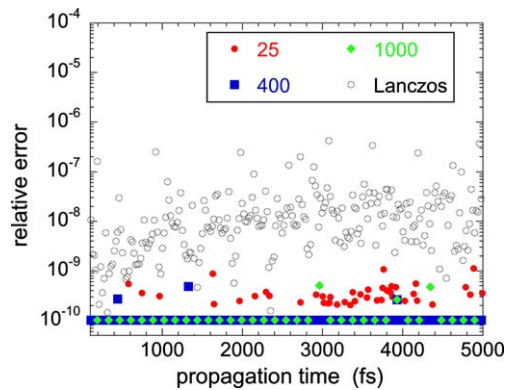


Fig. 3. Relative error (defined in the text) for the zero-order wave transmitted through the periodic layer of ionic crystal cylinders. Results obtained with the Faber propagation scheme (full symbols) and the Lanczos–Arnoldi scheme (open circles) are presented as a function of time measured in femtoseconds. The time step for the Lanczos–Arnoldi propagation is $\Delta t_L = 0.138$ fs. The time step for the Faber propagation scheme is given by $\Delta t_F = j\Delta t_L$, where the correspondence between different symbols and the values of j is indicated in the inset of the figure.

Table 1
Numerical costs and efficiency of the Faber polynomial propagation

Time step units of Δt_L	Number of $H\Psi$ operations		Computation time gain $\sim 2.5N_L/N_F$
	N_F (Faber)	N_L (Lanczos)	
25	170	175	2.5
50	290	350	3.0
100	525	700	3.3
200	980	1400	3.6
400	1890	2800	3.7
1000	4560	7000	3.8

significant digits in the calculated signal where found to coincide. The peaks correspond mainly to the instants of time when the oscillating electric field is close to zero. The gain in the propagation efficiency as compared to the Lanczos–Arnoldi scheme is twofold. First, a smaller number of actions of H on $\Psi(t)$ is needed to obtain $\Psi(t + \Delta t_F)$. In the Faber propagation scheme, it is given by the order of the Faber polynomial approximation of the fundamental solution, $N_F = n$. In the case of the Lanczos–Arnoldi scheme, the number of actions of H on $\Psi(t)$ is given by $N_L = K\Delta t_F/\Delta t_L$ where K is the dimension of the Krylov space. For the precision shown in Fig. 3, $K = 7$. Second, as we have already discussed in Ref. [12], for a typical size of the mesh as used here, computational costs of acting by H on $\Psi(t)$ are comparable with those of constructing an orthonormal basis for the Krylov space (by means of the Arnoldi process) and projecting the Hamiltonian onto the Krylov space (a $K \times K$ Hessenberg matrix for a non-Hermitian H). This explains an extra factor 2.5 in the fourth column of Table 1. For significantly larger sizes of the mesh, in particular, for 3D simulations, the computational costs of acting by H on Ψ should prevail, and the gain in the computation time should simply scale as N_L/N_F .

It is worth noting that memory requirements are lower for the present Faber propagation owing to the short recursion relation (associated with an elliptic contour). Indeed, in the case of the Lanczos–Arnoldi scheme the number of vectors to be kept in the operational memory equals K .

Finally, in the Lanczos–Arnoldi propagation scheme applied to the above system the time step Δt_L exceeds the Courant limit $\Delta t_C = \|H\|^{-1}$ at least in three times [12]. Therefore, the Faber propagation scheme allows one to exceed the Courant limit at least in 3000 times, $\Delta t_F \geq 3000 \Delta t_C$ as one can see from Table 1.

7. Conclusions

We have shown that the Faber propagation scheme can successfully be used in electrodynamics of passive media. The scheme is global in time, that is, it allows one for time steps that exceed the Courant limit in a few orders of magnitude. As a point of fact, the propagation can actually be carried out in a single time step if the system in question does not have long-lived quasistationary modes (as the structure resonance in the example we have considered above).

The essential virtue of the scheme is the exponential convergence, which leads to superior accuracy as compared to other time domain methods in passive media. The Faber propagation scheme can therefore be used as a benchmark, when comparing various propagation methods. If the medium is lossless and no absorber is present, the Faber scheme coincides with the Chebyshev propagation scheme, whose high accuracy is well known in time domain methods in computational quantum physics.

Another advantage of the present Faber propagation scheme is a relatively low memory demand. This, however, is essentially due to an elliptic contour which leads to a family of Faber polynomials that are generated by a short recursion relation. For example, the conventional leapfrog (time differencing) propagation scheme requires to have two arrays $\Psi(t)$ and $\Psi(t - \Delta t)$ in the operational memory to compute $\Psi(t + \Delta t)$, while in the Faber scheme associated with an elliptic contour, a recursive computation of the sum (1.3) requires storing three arrays $\Psi_m(t + \Delta t_F)$, Φ_m , and Φ_{m-1} , where Ψ_m is the series (1.3) with $k = 0, 1, \dots, m \leq n$, and $m = 1, 2, \dots, n$ being the recurrence running index, $\Psi_{m+1} = \Psi_m + c_{m+1}\Phi_{m+1}$. However, the gain of the Faber scheme in efficiency and accuracy is enormous.

It should be noted that we have not explored a further optimization of the present Faber propagation scheme because our main goal was to compare it with the Lanczos–Arnoldi propagation scheme (which was applied to the above system and shown to be more accurate and efficient than a typical finite differencing (leapfrog) scheme). For any application, the optimization should include the following. First, the spread of the spectrum along the real axis is essentially determined by the smallest grid spatial step. So, depending on the accuracy demand, E_m can be reduced. Second, the absorbing layer can also be optimized to reduce the spread v of the spectrum along the imaginary axis. In addition, one can try to estimate (e.g., by perturbation theory) imaginary parts of eigenvalues with large real parts (of order E_m). This would lead to a tighter ellipse. Finally, the contour shape itself can also be optimized, which, in general, requires a better knowledge of the spectrum of the Hamiltonian. Thus, for a specific problem on hands, the Faber propagation scheme can be made even more efficient than the simplest example presented in our work.

Acknowledgements

S.V.S. thanks the LCAM of the University of Paris-Sud and, in particular, Dr. V. Sidis for the support and warm hospitality extended to him during his stay in Orsay.

References

- [1] A. Taflove, S.C. Hagness, *Computational Electrodynamics – The Finite-difference Time-domain Method*, Artech House, Boston, MA, 2000.
- [2] S.H. Tseng, J.H. Greene, A. Taflove, D. Maitland, V. Backman, J. Walsh, *Opt. Lett.* 29 (2004) 1393; M.I. Mishchenko, G. Videen, V.A. Babenko, N.G. Khlebtsov, T. Wriedt, *J. Quant. Spectrosc. Radiat. Transfer* 88 (2004) 357, and references therein; K. Muinonen, *Waves Random Media* 14 (2004) 365.
- [3] G. Faber, *Math. Ann.* 57 (1903) 398; G. Faber, J. Reine, *Angew. Math.* 150 (1920) 79.
- [4] A.I. Markushevich, *Theory of Functions of a Complex Variable*, Chelsea, New York, 1977; V.L. Smirnov, N.A. Lebedev, *Functions of a Complex Variable: Constructive Theory*, MIT, Cambridge, 1968.
- [5] Y. Huang, W. Zhu, D.J. Kouri, D.K. Hoffman, *Chem. Phys. Lett.* 206 (1993) 96; *Chem. Phys. Lett.* 213 (1993) 209(E); Y. Huang, D.J. Kouri, D.K. Hoffman, *J. Chem. Phys.* 101 (1994) 10493.
- [6] W.T. Pollard, R.A. Friesner, *J. Chem. Phys.* 100 (1994) 5054.
- [7] W. Huisinga, L. Pesce, R. Kosloff, P. Saalfrank, *J. Chem. Phys.* 110 (1999) 5538.
- [8] H. Tal-Ezer, R. Kosloff, *J. Chem. Phys.* 81 (1984) 3967.
- [9] For a review of different propagation schemes for the time-dependent Schrödinger equation see: C. Leforestier, R.H. Bisseling, C. Cerjan, M.D. Feit, R. Friesner, A. Guldberg, A. Hammerich, G. Jolicard, W. Karrlein, H.-D. Meyer, N. Lipkin, O. Roncero, R. Kosloff, *J. Comput. Phys.* 94 (1991) 59, and references therein.
- [10] C. Cerjan (Ed.), *Numerical Grid Methods and Their Application to Schrödinger's Equation*, NATO ASI Series, Series C: Mathematical and Physical Sciences, vol. 412, Kluwer Academic Publishers, London, 1993.
- [11] H. De Raedt, K. Michielsen, J.S. Kole, M.T. Figge, *IEEE Trans. Antennas Propagat.* 51 (2003) 3155; *Phys. Rev. E* 67 (2003) 056706.
- [12] A.G. Borisov, S.V. Shabanov, *J. Comput. Phys.* 209 (2005) 643.
- [13] J.P. Boyd, *Chebyshev and Fourier Spectral Methods*, Springer-Verlag, New York, 1989.
- [14] D. Kosloff, R. Kosloff, *J. Comput. Phys.* 52 (1983) 35.
- [15] A. Rung, C.G. Ribbing, *Phys. Rev. Lett.* 92 (2004) 123901.
- [16] K.C. Huang, P. Bienstman, J.D. Joannopoulos, K.A. Nelson, S. Fan, *Phys. Rev. Lett.* 90 (2003) 196402.
- [17] S.V. Shabanov, *Electromagnetic pulse propagation in passive media by path integral methods*, a LANL e-preprint, 2003, Available from: <http://xxx.lanl.gov/abs/math.NA/0312296>.
- [18] A.G. Borisov, S.V. Shabanov, *J. Comput. Phys.* 199 (2004) 742.
- [19] T. Kövari, Ch. Pommerenke, *Math. Z.* 99 (1967) 193.
- [20] L.N. Trefethen, *SIAM J. Sci. Stat. Comput.* 1 (1980) 82.
- [21] G. Starke, R.S. Vagra, *Numer. Math.* 64 (1993) 213.
- [22] M.N. Spijker, *Appl. Numer. Math.* 13 (1993) 241.
- [23] S.W. Ellacott, *Math. Comput.* 40 (1983) 575.
- [24] K.O. Geddes, J.C. Mason, *SIAM J. Numer. Anal.* 12 (1975) 111.
- [25] E. Yablonovitch, *Phys. Rev. Lett.* 58 (1987) 2059; J.D. Joannopoulos, R.D. Meade, J.N. Winn, *Photonic Crystals*, Princeton University Press, Princeton, NJ, 1995; H.J. Lezec, A. Degiron, E. Devaux, R.A. Linke, L. Martin-Moreno, F.J. Garcia-Vidal, T.W. Ebbesen, *Science* 297 (2002) 820; T.W. Ebbesen, H.J. Lezec, H.F. Ghaemi, T. Thio, P.A. Wolff, *Nature (London)* 391 (1998) 667.
- [26] R.W. Wood, *Phys. Rev.* 48 (1935) 928.
- [27] R. Magnusson, S.S. Wang, *Appl. Phys. Lett.* 61 (1992) 1022; S. Peng, G.M. Morris, *Opt. Lett.* 21 (1996) 549; T. Peter, R. Bräuer, O. Bryngdahl, *Opt. Commun.* 139 (1997) 177; K. Koshino, *Phys. Rev. B* 67 (2003) 165213; L. Piloizzi, A. D'Andrea, R. Del Sole, *Phys. Rev. B* 54 (1996) 10763.
- [28] A.G. Borisov, F.J. García de Abajo, S.V. Shabanov, *Phys. Rev. B* 71 (2005) 075408.
- [29] L.-S. Chen, C.-H. Kuo, Z. Ye, *Phys. Rev. E* 69 (2004) 066612; E. Chow, S.Y. Lin, S.G. Johnson, P.R. Villeneuve, J.D. Joannopoulos, J.R. Wendt, G.A. Vawter, W. Zubrzycki, H. Hou, A. Alleman, *Nature* 407 (2000) 983.